Fundamental Research 2 (2022) 66–73

Contents lists available at ScienceDirect

Fundamental Research

journal homepage: http://www.keaipublishing.com/en/journals/fundamental-research/

Article

Generation of singlet oxygen via iron-dependent lipid peroxidation and its role in Ferroptosis

Xiaofei Zhang[a,b,c], Lie Wu[a,*], Wenyao Zhen[a,b], Shanshan Li[a,b], Xiue Jiang[a,b,*]

[a] State Key Laboratory of Electroanalytical Chemistry, Changchun Institute of Applied Chemistry, Chinese Academy of Science, Changchun, Jilin 130022, China
[b] Graduate School of University of Science and Technology of China, Anhui 230026, China
[c] Changchun University, Changchun, Jilin 130022, China

ARTICLE INFO

Article history:
Received 29 April 2021
Received in revised form 30 June 2021
Accepted 1 July 2021
Available online 9 August 2021

Keywords:
Ferroptosis
Lipid peroxidation
Singlet oxygen
Russell mechanism

ABSTRACT

Ferroptosis is a cell death pathway mediated by iron-dependent accumulation of lipid peroxide. However, the specific downstream molecular events of iron-dependent lipid peroxidation are yet to be elucidated. In this study, based on various spectral analyses, we have found evidence that singlet oxygen is produced through the Russell mechanism during the self-reaction of lipid peroxyl radicals generated via iron-dependent lipid peroxidation regardless of the presence of cholesterol. Significantly reduced generation of singlet oxygen was observed in the absence of iron. The generated singlet oxygen accelerated the oxidative damage of lipid membranes by propagating lipid peroxidation and facilitated ferroptotic cancer cell death initiated by erastin. In this work, singlet oxygen has been revealed to be a new reactive species that participates in ferroptosis, thus improving the understanding on iron-dependent lipid peroxidation and the mechanism of ferroptosis.

1. Introduction

As a common biological phenomenon, cell death plays a central role in various biological processes and in the pathogenesis and progression of diseases. Cell death is usually categorized into accidental and regulated cell death; the former is a biologically uncontrolled process, whereas the latter is a genetically programmed cellular process induced by severe physical, chemical, or mechanical stimulation, as well as genetic and pharmacological perturbation [1]. Ferroptosis, which is different from apoptosis, necrosis, and autophagy, is a type of regulated cell death induced by iron-dependent lipid peroxidation under the regulation of multiple metabolic processes involving amino acids and lipids [2, 3]. As it is a lipid-peroxidation-based cell death, modulation of the produced lipid reactive oxygen species (ROS) can significantly affect ferroptosis. For example, ferroptosis can be induced by the inhibition of the transmembrane cysteine/glutamate antiporter system Xc^-. Inhibition of the system Xc^- has a negative effect on the synthesis of glutathione (GSH), a cofactor of glutathione peroxidase 4 (GPX4), resulting in the indirect inactivation of GPX4. This causes an increase in cytosolic and lipid ROS, triggering ferroptosis [4, 5]. Similarly, activation of the P53 gene provides an alternative route to ferroptosis by inhibiting both the uptake of cysteine by the system Xc^- and the synthesis of GSH [6]. In addition, direct inhibition of the activity of GPX4 by small molecule inhibitors can also initiate ferroptosis [7]. More recently, ferroptosis suppressor protein 1 (FSP1) and GTP cyclohydrolase 1 have been found to exhibit a protective effect against ferroptosis by the indirect reduction of lipid radicals via redox mediators [8].

In addition to understanding the elimination of lipid peroxides, elucidation of the mechanism by which it is generated is another challenge in gaining insight into the molecular mechanism of ferroptosis. Lipid peroxides can be produced enzymatically or nonenzymatically [9, 10]. When lipid hydroperoxides are generated enzymatically, the peroxidation of polyunsaturated fatty acids (PUFAs) by iron-containing lipoxygenases plays a major role in ferroptosis [11]. Esterified arachidonoyl or adrenoyl species can act as substrates for lipoxygenases. In the presence of insufficient GPX4, the lipoxygenase-catalyzed reaction leads to the accumulation of lipid hydroperoxides [12], which can be decomposed into various lipid ROS [10]. The nonenzymatic pathway of lipid peroxidation can be initiated by iron-dependent Fenton chemistry [13]. PUFAs are susceptible to hydrogen abstraction (e.g., induced by hydroxyl radicals), producing alkyl radicals and subsequently peroxyl radicals (via molecular oxygen reactions), which can continuously propagate by reacting with the proximal PUFAs [9, 14]. In addition, enzymatically produced lipid hydroperoxides can react with iron cations to generate peroxyl or alkoxyl radicals, resulting in the propagation of lipid peroxidation [15]. However, the detailed metabolic mechanism for the generation of lipid ROS remains elusive.

* Corresponding authors.
E-mail addresses: lwu@ciac.ac.cn (L. Wu), jiangxiue@ciac.ac.cn (X. Jiang).

https://doi.org/10.1016/j.fmre.2021.07.008

Howard et al. found that singlet oxygen ($^1O_2$) can be generated through the self-recombination of two peroxyl radicals by the Russell mechanism [16]. As the lipid peroxyl radical (ROO•) is one of the predominant intermediates during the propagation of lipid peroxidation, $^1O_2$ could be generated during lipid ROS metabolism. $^1O_2$ has a higher oxidizing potency than lipid ROS [17, 18], which may accelerate lipid peroxidation, produce more lipid ROS, and further promote ferroptosis. However, the mechanism for generating $^1O_2$ and its potential role in ferroptosis are not clearly understood. In this study, we investigate the highly iron-dependent generation of $^1O_2$ through the Russell mechanism and its role in the propagation of lipid peroxidation initiated by Fenton chemistry in the presence of cholesterol, which further promotes the propagation of lipid peroxidation and intensifies erastin-induced ferroptotic cell death, thus providing new insights into the molecular mechanism of ferroptosis and related disease therapies.

2. Methods

2.1. Preparation of liposomes

Liposomes containing pure lipids or lipid/cholesterol mixtures were prepared by hydration and sonication. To prepare liposomes containing pure lipid, a given quantity of lipid (1 mg) was dissolved in chloroform in a glass vial, whereas to prepare liposomes containing lipid and cholesterol, lipids were mixed with cholesterol at a molar ratio of 7:3 in chloroform. Chloroform was removed by using a nitrogen stream to form a dry lipid film on the wall of the glass vial, which was then kept under vacuum for at least 5 h. The dried lipid film was hydrated and resuspended from the wall of the vial in phosphate buffer (5 mM, pH 5.5) or H_2O to yield a final concentration of 1 mg/mL through vigorous vortexing. The cloudy solution was tip-sonicated until the solution became clear. Sonication was performed on a 40% duty cycle (3 s on followed by 5 s off) in a cold bath to avoid oxidation of the lipids. Finally, the clear liposome solution was centrifuged at 11,000 rpm for 20 min to remove any metal particles.

2.2. Detection of $^1O_2$ generation during lipid peroxidation

Singlet oxygen sensor green (SOSG) is highly sensitive to $^1O_2$ and is generally used to detect the generation of $^1O_2$. To detect $^1O_2$ generation during •OH-induced lipid peroxidation, 100 μL liposome solution (1 mg/mL), 10 μL 0.5 mM $FeCl_2$, 6 μL 0.5 mM H_2O_2, and 10 μL SOSG solution (1 mM dissolved in dimethylsulfoxide (DMSO)) were mixed in 874 μL of phosphate buffer (5 mM, pH 5.5) for 60 min, and the fluorescence of SOSG was recorded. In addition, the fluorescence of SOSG in phosphate buffer containing only liposomes, $FeCl_2$, and H_2O_2 was also measured under the same conditions as a control experiment. For fluorescence measurement, SOSG was excited at 490 nm, and the emission was recorded over 500–650 nm. The slit width was set to 3 nm during excitation and emission. For the detection of $^1O_2$ generation from the products of $^1O_2$-induced lipid peroxidation, 100 μL liposome solution (1 mg/mL) was added to a quartz cuvette containing 900 μL methylene blue (MB) aqueous solution (6 μg/mL) and irradiated for 40 min using a 650 nm laser (1 Wcm^{-2}). Then, 100 μL of the obtained solution was mixed with 25 μL 0.5 mM $FeCl_2$ or Fe^{2+}-EDTA solution (0.5 mM) and 10 μL SOSG solution (1 mM dissolved in DMSO) in 865 μL phosphate buffer (5 mM, pH 5.5) for 60 min, and the fluorescence of SOSG was recorded. In addition, the fluorescence of SOSG in phosphate buffer (5 mM, pH 5.5) containing either a mixture of liposomes or MB irradiated by a laser under the same conditions was also measured.

2.3. Detection of •OH from Fenton reaction

The generation of •OH was detected by the degradation of MB. For the detection of low-concentrations of •OH from the Fenton reaction, 10 μL H_2O_2 (0.3 mM) was added to 990 μL phosphate buffer (5 mM, pH 5.5) containing MB (10 μg/mL) and $FeCl_2$ (5 μM) or $FeCl_2$ + EDTA•2Na (5 μM) to initiate the generation of •OH. The reaction was allowed to continue for 60 min. Subsequently, the absorption spectrum of MB was recorded. The UV–vis spectrum of MB was measured with a background spectrum of phosphate buffer (5 mM, pH 5.5). To detect high concentrations of •OH from the Fenton reaction, 10 μL H_2O_2 (6 mM) was added to 990 μL phosphate buffer (5 mM, pH 5.5) containing MB (10 μg/mL) and $FeCl_2$ + EDTA•2Na (100 μM).

2.4. Detection of lipid peroxidation products by mass spectroscopy

For detection of the products of •OH-induced lipid peroxidation, an aqueous solution (100 μg/mL) of dioleoyl-glycero-phosphoserine (PS) or dioleoyl-glycero-phosphoserine/cholesterol (PS/Ch) liposomes was incubated for 60 min with 62.5 μM $FeCl_2$ and 37.5 μM H_2O_2. Thereafter, 100 μL of the aforementioned mixture was injected into a tandem mass spectrometer. An electrospray ionization source and the negative ion detection mode were used to detect the peroxidation products of PS, whereas an atmospheric pressure chemical ionization source and the positive ion mode were used to detect the peroxidation products of Ch. To detect the products of PS lipid peroxidation induced by $^1O_2$ generated via the irradiation of MB, 100 μL liposome solution (1 mg/mL) was added to a quartz cuvette containing 100 μL MB (6 μg/mL), and irradiated for 40 min using a 650 nm laser (1 Wcm^{-2}). Then, 100 μL of the obtained solution was injected into a tandem mass spectrometer.

2.5. Surface-enhanced infrared absorption (SEIRA) spectroscopy to record changes in lipid membranes caused by the Fenton reaction

The supported lipid membrane equilibrated in phosphate buffer (5 mM, pH 5.5) for a given time was used to record the reference spectrum. Sample spectra were recorded for 5 min at intervals of 60 s while adding $FeCl_2$ solution to reach a final concentration of 62.5 μM to monitor the Fe^{2+}-induced structural changes in the membrane. A new reference spectrum was recorded after further equilibration, and the sample spectra were measured while adding H_2O_2 with or without NaN_3. The final concentrations of H_2O_2 and NaN_3 were 37.5 μM and 25 μM, respectively.

2.6. Detection of singlet oxygen by SOSG in living cells

A549 cells were seeded into culture dishes (2×10^5 cells per dish) and cultured for 24 h. The cells were thoroughly and carefully washed with phosphate-buffered saline (PBS) solution multiple times to remove the proteins in the culture dishes as well as the proteins adsorbed on the cell surfaces. Then, 1 mL 5 μM SOSG (dissolved in dulbecco's modified eagle medium (DMEM)) was added to the cells and they were incubated for 30 min in DMEM to incorporate the SOSG probes. The cells were rinsed three times with PBS after the incorporation of SOSG probes. Stained cells were cultured with erastin (100 μM in DMEM) with or without NaN_3 (100 μM in DMEM) for another 8 h. After rinsing three times with PBS, the cells were imaged using a confocal laser scanning fluorescence microscope (CLSM) at an excitation wavelength of 488 nm, and the emission was recorded between 500 and 570 nm. Stained cells incubated with the same amount of DMSO that was introduced upon adding erastin or NaN_3 were also imaged as a control.

2.7. Cell viability assay

A549 cells were seeded into 96-well plates (5×10^3 cells per well) and cultured for 24 h. To determine the cell viability after treatment with erastin, cells were cultured with erastin (6, 20, 40, 60, and 100 μM in DMEM, respectively) for another 24 h. To investigate the effect of deferoxamine mesylate (DFO) on erastin-induced cell death, cells were cultured with erastin (40 μM and 60 μM in DMEM) with or without DFO (100 μM in DMEM) for 24 h, and cells cultured with DFO (100 μM in

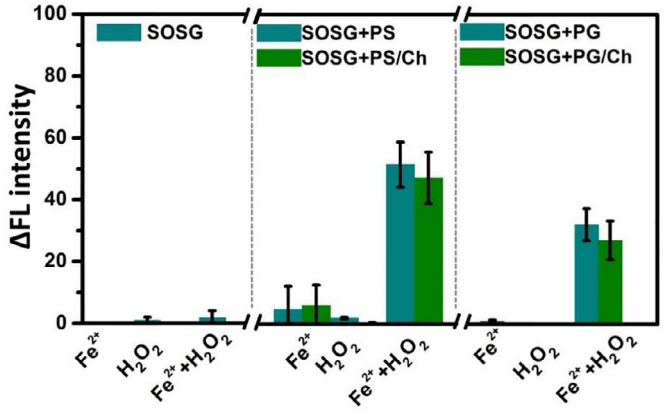

Fig. 1. Singlet oxygen ($^1O_2$) generated during the reaction of Fenton reagent (5 μM Fe^{2+} and 3 μM H_2O_2) with various liposomes (100 μg/mL) in phosphate buffer (5 mM, pH 5.5). Generation of $^1O_2$ was detected by the specific probe, singlet oxygen sensor green (SOSG), and quantified based on the changes in emission intensity at 525 nm from at least three independent measurements. PS: dioleoyl-glycero-phosphoserine liposomes; PS/Ch: dioleoyl-glycero-phosphoserine/cholesterol liposomes; PG: dioleoyl-glycero-phosphoglycerol liposomes; PG/Ch: dioleoyl-glycero- phosphoglycerol/cholesterol liposomes.

DMEM) alone were treated as control groups. To investigate the effect of singlet oxygen on erastin-induced cell death, cells were cultured with erastin (20 μM and 40 μM in DMEM) with or without NaN_3 (100 μM in DMEM) for 24 h, and cells cultured with NaN_3 (100 μM in DMEM) alone were treated as control groups. For all cases, cells cultured with the same amount of DMSO that was introduced by adding erastin, DFO, or NaN_3 were imaged as controls. Subsequently, cells were washed with PBS, and 200 μL methylthiazolyldiphenyl-tetrazolium bromide (MTT) (0.5 mg/mL) dissolved in PBS was added to each well. After culturing for another 4 h, PBS was replaced with DMSO (100 μL) and the 96-well plates were shaken for 10 min to dissolve the generated blue formazan. Finally, a microplate reader was used to measure the absorbance of each well at 570 nm. Cell viability was determined by the following equation: cell viability (%) = (average absorbance value of treatment group/average absorbance value of control group) × 100% and expressed as a percentage histogram.

3. Results and discussion

3.1. Investigating the generation of singlet oxygen during lipid peroxidation induced by the Fenton reaction

Dioleoyl-glycero-phosphoserine (PS) was selected as a model lipid to explore whether lipid peroxidation during ferroptosis would produce $^1O_2$, because PS lipid is one of the essential components of healthy nerve cell membranes, and a decrease in the PS content of the membranes would lead to functional impairment of nerve cells [19]. It has been reported that the unsaturated PS lipid content decreases significantly during ferroptosis [20]. Therefore, elucidation of the molecular mechanism of PS lipid peroxidation would be beneficial for understanding the underlying mechanisms of ferroptosis and degenerative diseases. The peroxidation of PS lipids was triggered by hydroxyl radicals (•OH) produced from the Fenton reagent (a mixture of iron cations and hydrogen peroxide). SOSG, a specific $^1O_2$ probe, was used to detect the generation of $^1O_2$ during this process. As shown in Figs. 1 and S1, the fluorescence intensity of SOSG increases upon the addition of Fenton reagent to PS liposomes relative to that obtained by the individual addition of iron cations or H_2O_2, and its intensity remains nearly unchanged under identical conditions in the absence of PS liposomes, indicating that $^1O_2$ is generated during •OH-induced PS lipid peroxidation. In addition to phospholipids, cholesterol (Ch) plays an important role in maintaining the structure and function of biomembranes. Previously, it has been reported that Ch can non-sacrificially protect membrane lipids from oxidative damage caused by •OH by increasing the order of the membranes [21]. However, according to other reports, Ch itself is susceptible to free radical species and non-radical ROS, and can be oxidized into oxysterols [22]. To investigate the potential effect of Ch on the generation of $^1O_2$ during PS lipid peroxidation, Ch and PS lipids were mixed at a molar ratio of 3:7 to form PS/Ch liposomes. Notably, an increase in the fluorescence intensity of SOSG was observed upon the addition of Fenton reagent to the PS/Ch liposome solution, although it was slightly weaker than that for standalone PS liposomes, suggesting that $^1O_2$ can be generated in the presence of Ch. Similar phenomena were observed (Fig. 1) when PS lipids were substituted with dioleoyl-glycero-phosphoglycerol (PG) lipids with nearly the same negative charge (Fig. S2). This further demonstrates that Ch has negligible effect on the generation of $^1O_2$ during •OH-induced lipid peroxidation, although it was reported that Ch exhibits a sacrificial or non-sacrificial protective effect on lipids against chemical damage [21-22], caused by the reduced effect of Ch on the order of PS lipid membranes at the membrane-aqueous interface (detailed discussions are presented in Figs. S3 and S4). These results indicate that $^1O_2$ is generated during •OH-induced lipid peroxidation regardless of the presence of Ch.

3.2. Investigating the mechanism of singlet oxygen generation in lipid peroxidation induced by Fenton reaction and its dependence on iron cations

The results indicate that •OH, as the most potent ROS, is capable of initiating lipid peroxidation through its strong hydrogen abstraction ability [13, 23]. The reaction might begin with the abstraction of an allylic hydrogen from the unsaturated lipid by •OH [24]. The resulting allylic radical (R•) can then couple with molecular oxygen (O_2) to yield a peroxyl radical (ROO•), which can react further with surrounding lipids to produce lipid hydroperoxides (R-OOH) and alkyl radicals (R•). The latter can react with oxygen to produce peroxyl radicals (ROO•), resulting in the propagation of lipid peroxidation and the accumulation of lipid ROS [8-9, 15, 23]. Thus, it can be postulated that $^1O_2$ is generated from two ROO• radicals formed during lipid peroxidation through the Russell mechanism [25] accompanied by oxidation products with hydroxyl and carbonyl groups (named as R-OH and $R=O$, respectively). To validate the proposed $^1O_2$ production pathway, the products resulting from the interaction between PS liposomes and the Fenton reagent were analyzed by using mass spectrometry (MS) in the negative-ion mode. Peaks at m/z 786.52, 800.44, 802.54, and 818.47 were observed in the primary MS (Fig. 2(A)) and their respective daughter ions with m/z of 699.66, 713.56, 715.61, and 731.51 were observed in the secondary MS, (Figs. S5(A)–(D)). As the -CH_2CHNH_2COO- fragment (with a molecular weight of 87) at the lipid head group was reported to be frequently lost in tandem MS analysis [26], the peak at m/z 786.52 was assigned to the PS parent anion [27]. Peaks at m/z 800.44, 802.54, and 818.47 were assigned to the PS derivatives formed via the addition of carbonyl (PS=*O*), hydroxyl (PS-OH), and hydroperoxide (PS-OOH), respectively. Fig. S6 shows the potential reaction pathways and products with the calculated exact masses. The occurrence of PS=*O* (at m/z 800.44), PS-OH (at m/z 802.54), and PS-OOH (at m/z 818.47) supports the proposed reaction pathway in which $^1O_2$ is generated from two radicals (ROO•) through the Russell mechanism during •OH-mediated lipid peroxidation.

It should be noted that at the lower m/z end, a peak appeared at m/z 692.58 (Fig. 2(A)) with that of its daughter ion at m/z 605.45 (Fig. S5(E)) were observed, which were assigned to the product resulting from the formylation of PS accompanied by the cleavage of some tail alkyl chains via addition chemistry [28]. This suggests the occurrence of •OH-mediated oxidation via addition chemistry under experimental conditions. The observed peaks at m/z 802.54 and 818.47 could also be assigned to PS oxidation products resulting from the addition of one and two carbonyl groups (+16 Da and +32 Da), respectively, to the par-

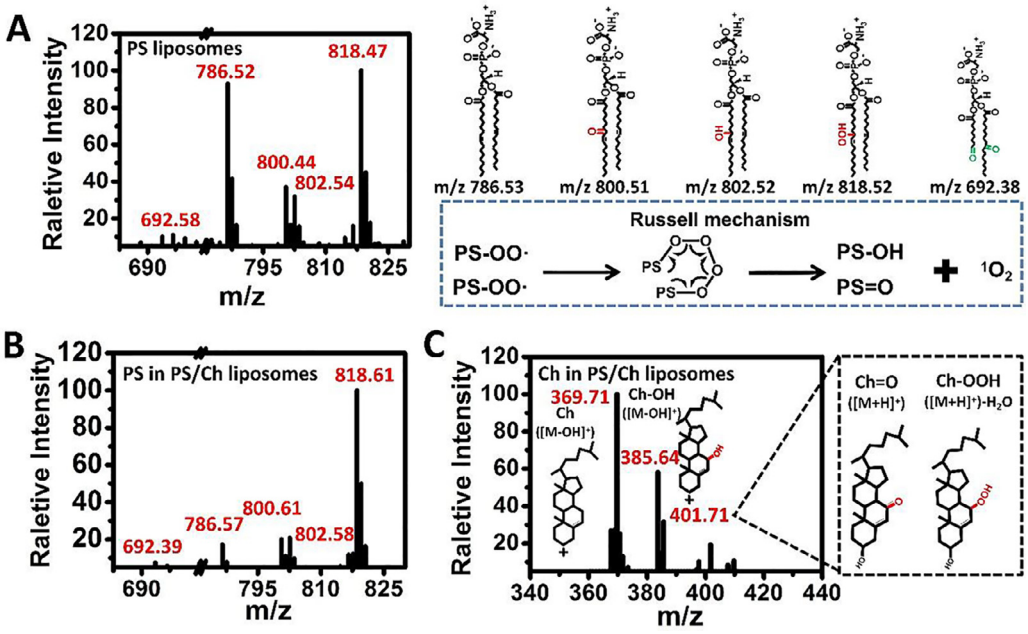

Fig. 2. Mass spectra of products from the reaction of Fenton reagent (62.5 μM Fe^{2+} and 37.5 μM H_2O_2) with liposomes (100 μg/mL). (A) Mass spectra of PS liposomes after interacting with Fenton reagent (left panel), and proposed product structures from Russell reaction; (B, C) Mass spectra of PS/Ch liposomes after interacting with Fenton reagent. (B) PS related products, and (C) Ch related products.

ent PS ion during oxidation by •OH via addition chemistry (Figs. S5(C) and (D) and Fig. S6 (pathway II)). As free radical-mediated lipid peroxidation is a rather complex process [23], it is possible that HO-ROO• generated through addition chemistry may generate $^1O_2$ via the Russell mechanism. Therefore, the detailed molecular mechanism of $^1O_2$ generation during •OH-mediated lipid peroxidation remains open for investigation. However, our results clearly suggest that $^1O_2$ is generated through the Russell mechanism from two ROO• radicals formed during lipid peroxidation, as evidenced by the simultaneous observation of key intermediates (PS-OOH at *m/z* 818.47) and final products (PS=*O* at *m/z* 800.44 and PS-OH at *m/z* 802.54). Further investigation and identification of the radicals involved using electron spin resonance measurements combined with radical trapping techniques might provide more valuable information and evidence for the underlying molecular mechanism.

For the products formed upon the reaction of PS/Ch liposomes with Fenton reagent, a similar peak pattern was observed in both the primary (Fig. 2(B)) and secondary MS (Figs. S7(A)–(D)), suggesting that the peroxidation products of PS in PS/Ch liposomes included PS-OOH, which underwent subsequent reactions through the Russell mechanism, leading to the PS=*O* and PS-OH products. This proves that the incorporation of Ch has negligible effect on the peroxidation of PS lipids and the subsequent Russell reaction. Products related to Ch in PS/Ch liposomes were analyzed in the positive-ion mode. The peak observed at *m/z* 369.71 (Fig. 2(C)) was reported to be a marker of Ch in MS, which was assigned to the pseudo-molecular ion of Ch ($[M\text{-}OH]^+$) [29]. The occurrence of its oxidation product at *m/z* 385.64 indicates the presence of a hydroxyl oxidation product (Ch-OH), as proved by the fragment with *m/z* 367.43 in the secondary MS (Fig. S7(E)), resulting from the loss of molecular H_2O [30]. In addition, the peak at *m/z* 401.71 may have originated from the protonated carbonyl oxidation product of Ch (Ch=*O*) and/or hydroperoxide of Ch (Ch-OOH) but the later was accompanied with the loss of molecular H_2O [30–31]. The consecutive loss of H_2O molecules was confirmed by the presence of peaks at *m/z* 383.41 and 365.49 in the secondary MS of the product corresponding to the *m/z* 401.71 peak (Fig. S7(F)). This lends further support to the assignment of *m/z* 401.71 to Ch-OOH. These results indicate that the peroxidation products of Ch formed through reaction with Fenton reagent might contain Ch-OOH and Ch=*O*. The peroxidation of Ch would consume the •OH produced by the Fenton reagent, thus inhibiting lipid peroxidation. Ch peroxides incorporated in liposomes might have less opportunity for direct contact with each other and thus generate $^1O_2$. This might be responsible for the observed slight reduction in the total amount of $^1O_2$ generated upon Ch incorporation (PS/Ch liposomes).

MS results suggest that $^1O_2$ is generated through the Russell mechanism from two PS-OO• radicals, and the key intermediate PS-OOH was observed. However, PS-OO• might have originated via two pathways (Fig. 3(A)). PS-OO• can be directly generated during •OH-mediated peroxidation (Fig. 3(A), blue arrow, and Fig. S6). It was also reported that R-OOH pre-formed in lipid peroxidation could be further cleaved by catalytically active iron cations, forming more reactive species, such as ROO•, alkoxyl (RO•), and epoxyperoxyl radical (OROO•) [15–16, 25, 32]. These species can abstract H-atoms from lipids to propagate the peroxidation chain reaction. Thus, PS-OO• can be produced through an iron cation-dependent chain reaction pathway (Fig. 3(A), pink arrow). To further identify the molecular mechanism of $^1O_2$ generation and the function of iron cations, the interaction between iron cations and PS/PS-OOH mixed liposomes was investigated. PS-OOH was generated by oxidizing PS liposomes with $^1O_2$ generated from the photosensitizer MB under illumination with a 650 nm laser in a mixed solution [25]. The successful production of PS-OOH was further confirmed by the peak at *m/z* 818.53 and its fragment at *m/z* 731.49 in MS analysis (Fig. S8). SOSG was added to the resultant PS/PS-OOH mixed liposomes, and its fluorescence intensity was recorded as a reference to eliminate the influence of any residual $^1O_2$ generated from MB. The increase in the fluorescence intensity of SOSG after addition of Fe^{2+} suggests the generation of $^1O_2$ due to the interaction between Fe^{2+} and PS/PS-OOH liposomes (Fig. 3(B)). Furthermore, when Fe^{2+} was pre-chelated with equivalent molar EDTA (Fe^{2+}-EDTA), nearly no $^1O_2$ was generated, as evidenced by the negligible change in the fluorescence intensity of SOSG (Fig. 3(B)), indicating that Fe^{2+}-EDTA significantly reduces the catalytic activity of iron cations toward the decomposition of lipid hydroperoxide because of the failure of chelated iron cation to be in close proximity to the reactive PS-OOH [32]. These results indicate that $^1O_2$ is generated from the self-reaction of the neighboring PS-OO• produced from the decomposition of PS-OOH by iron cations and the resultant

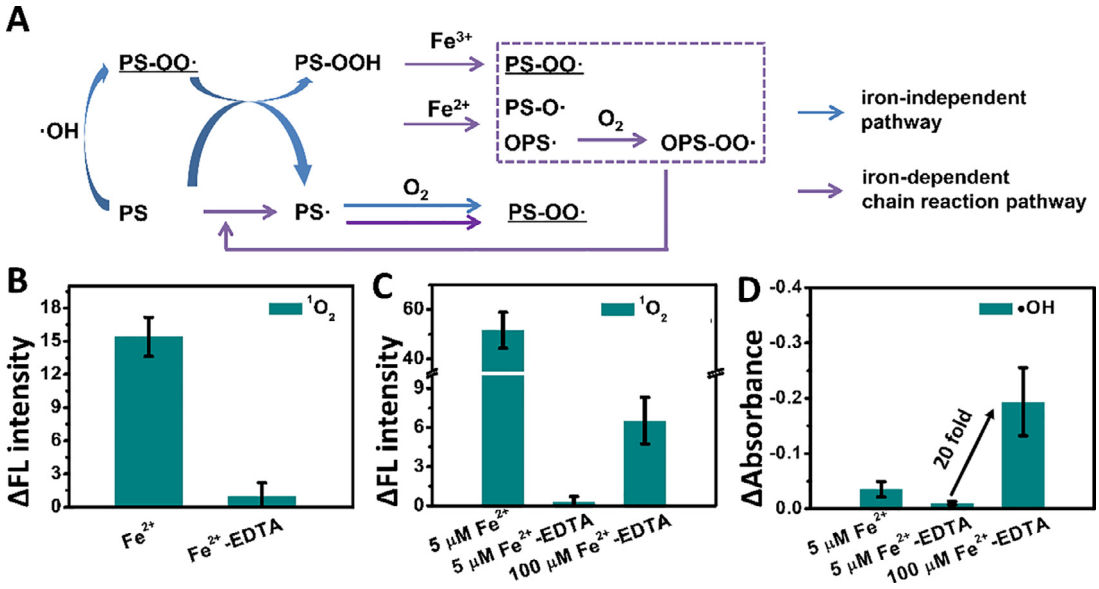

Fig. 3. (A) Schematic of pathways for $^1O_2$ generation in •OH-induced lipid peroxidation. (B) Generation of $^1O_2$ (as detected by SOSG) from reaction between PS/PS-OOH liposomes (100 μg/mL) and Fe^{2+} (12.5 μM) or Fe^{2+}-EDTA (12.5 μM). (C) Generation of $^1O_2$ (as detected by SOSG) from reaction between PS liposomes (100 μg/mL) and different Fenton reagents (5 μM Fe^{2+} or Fe^{2+}-EDTA with 3 μM H_2O_2, and 100 μM Fe^{2+}-EDTA with 60 μM H_2O_2). (D) Generation of •OH from corresponding Fenton reagents as detected by degradation of MB. The production of $^1O_2$ and •OH was quantified based on the changes in emission intensity of SOSG at 525 nm and the changes in absorption of MB at 665 nm from at least three independent measurements.

chain reaction. As Fe^{2+}-EDTA complex could induce Fenton chemistry [13], it could serve as an inhibitor of iron cation-dependent PS-OOH decomposition, thus enabling distinction between the contributions of the self-reaction of the neighboring PS-OO• produced directly from •OH-mediated peroxidation and the iron-ion-dependent decomposition of PS-OOH and the resultant chain reaction (Fig. 3(A)) to $^1O_2$ generation. As shown in Fig. 3(C), replacing Fe^{2+} in the Fenton reagent with Fe^{2+}-EDTA results in no noticeable $^1O_2$ generation. Although the amount of • OH produced by the Fe^{2+}-EDTA system was less than that produced by the Fe^{2+} system (Fig. 3(D)), such a change cannot account for the dramatic difference in $^1O_2$ production. Although the production of •OH was significantly (20-fold) enhanced upon increasing the concentrations of Fe^{2+}-EDTA and H_2O_2 (Fig. 3(D)), the amount of $^1O_2$ generated was much less than that induced by Fenton reagent containing Fe^{2+} at a concentration that was only one twentieth of that of Fe^{2+}-EDTA (Fig. 3(C)). These results suggest that only a small amount of $^1O_2$ can be produced directly from •OH-mediated peroxidation, whereas a large amount of $^1O_2$ results from the self-reaction of two peroxy radicals produced by the iron cation-dependent decomposition of PS-OOH and the resultant propagation of the lipid peroxidation chain reaction.

3.3. Identifying the effect of produced singlet oxygen on membrane integrity and cellular activity

In addition to the •OH generated from the Fenton reagent, lipid peroxidation could also be induced by $^1O_2$. Therefore, the generation of $^1O_2$ might strengthen the propagation of lipid ROS. To examine this possibility, oxidation of the fluorescent probe C11-BODIPY in liposomes exposed to Fenton's reagent was performed, and NaN_3 was applied as a specific quencher of $^1O_2$ [25]. C11-BODIPY is sensitive to a variety of oxy-radicals and can be oxidized not only by the oxidation-initiating species but also lipid ROS during the chain-propagation process [33]. Thus, C11-BODIPY can be used to report the total ROS content around the membranes. The fluorescence intensity of C11-BODIPY decreased owing to the generation of •OH by the Fenton reagent around the membranes and the generated $^1O_2$ during the iron-dependent peroxidation of PS liposomes by •OH, and the resulted lipid ROS induced by •OH and $^1O_2$ (Fig. S9(A)). However, in presence of NaN_3, the fluorescence intensity was restored by approximately 20% (based on the changes in emission intensity at 591 nm), indicating that the generation of membrane-related ROS is reduced in presence of the $^1O_2$ quencher. This further supports the conclusion that $^1O_2$ is generated by •OH-induced lipid peroxidation. The alleviated oxidation of C11-BODIPY was due to $^1O_2$ and lipid ROS generated from the $^1O_2$-induced oxidation. The same phenomenon was observed for the peroxidation of PS/Ch liposomes by •OH (Fig. S9(B)). These results suggest that $^1O_2$ generated during the oxidation of PS and PS/Ch liposomes by Fenton reagent contributes to the total ROS content of the membrane in addition to •OH, which may accelerate the loss of lipid membrane integrity.

To investigate the damaging effects of $^1O_2$ and lipid ROS on the lipid membranes, surface-enhanced infrared absorption (SEIRA) spectroscopy was performed to monitor the Fenton reagent-induced structural changes in solid-supported PS and PS/Ch lipid membranes (Figs. S3 and S4) in the presence and absence of NaN_3. Figs. 4(A-a) and (B-a) show characteristic peaks of the prepared PS and PS/Ch membranes. The detailed peak assignments are shown in Fig. S3. Notably, regardless of the presence of Ch, the peak corresponding to υ_{as} (CH_2) for the PS lipid was located at 2927 cm^{-1}, that is, at a frequency value higher than that of the corresponding vibration for a highly ordered 1-dodecanethiol monolayer (at 2921 cm^{-1}). This suggests that the packing of PS in the membrane is relatively loose, and the presence of Ch does not have any significant effect on the order of the PS membrane. The absorption intensities of the peaks corresponding to υ_s (PO_2^-) and υ (P-O-C) of the phosphate groups exhibited a certain difference between the PS and PS/Ch membranes, suggesting that the presence of Ch changes the conformation of the phosphate groups of PS to a certain extent. It has been reported that the order of the lipid membrane has a dramatic effect on the degree and mechanism of radical-induced oxidation of membranes, loose packing typically results in the oxidation of the membrane by •OH through addition chemistry [28]. Our results are consistent with this report, and further indicate that incorporation of Ch has less effect on oxidation because of its negligible effect on membrane ordering.

When the PS membrane was immersed in phosphate buffer (5 mM, pH 5.5) as a reference, positive peaks in the υ (CH_2) region (2925 and 2855 cm^{-1}), as well as two peaks at 1738 (–)/ 1715 (+) cm^{-1} assigned to the υ ($C=O$) of the ester group in the alkyl chain of PS were observed

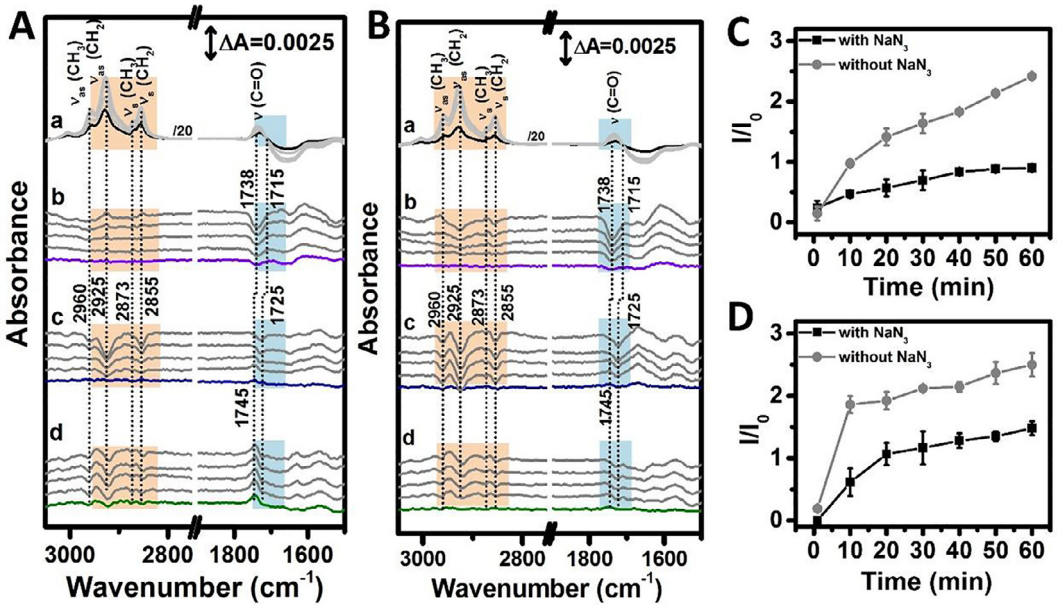

Fig. 4. (A, B) SEIRA difference spectra of PS (A) and PS/Ch (B) lipid membrane in phosphate buffer (5 mM, pH 5.5). (a) Lipid membrane formation with hydrophobic 1-dodecanethiol monolayer as background; (b) Fe^{2+}-induced structural changes in lipid membrane using membrane immersed in phosphate buffer (5 mM, pH 5.5) as reference; (c) Fenton reagent-induced structural changes in lipid membrane using membrane in presence of $FeCl_2$ as reference; H_2O_2 was further added for the purpose of comparison with (b) and the structural changes induced were recorded; (d) Fenton reagent with NaN_3-induced structural changes in lipid membrane using membrane in presence of $FeCl_2$ as a reference; mixed solution of H_2O_2 and NaN_3 was added instead of pure H_2O_2 in (c), and the structural changes induced were recorded. (C, D) Peroxidation damage of PS membrane (C) and PS/Ch membrane (D) presented by the time-dependent absolute value of intensity ratio (I/I_0) of υ_{as} (CH_2) before (I_0, positive peak) and after (I, negative peak) membrane peroxidation.

in the SEIRA difference spectra upon the addition of $FeCl_2$ (Fig. 4(A-b)). The carboxyl in the head group of PS is deprotonated under the experimental conditions (pH 5.5) [34]. The potential binding of metal ions would result in a difference in the peak positions of the carboxylate [35]. Thus, the two peaks at 1738 (−)/1715 (+) cm^{-1} were assigned to the υ ($C=O$) of the ester group in the alkyl chain, which might have resulted from the slight conformational change in the hydrocarbon chain due to the interaction of iron ions with lipids. However, negative peaks at 2925 and 2855 cm^{-1} were observed for the PS/Ch membrane (Fig. 4(B-b)), indicating that the addition of Fe^{2+} induces a different conformational change in the PS hydrocarbon chain in the presence of Ch. This proves the successful incorporation of Ch into PS membranes. After interacting with $FeCl_2$ for 60 min, the spectrum of PS or PS/Ch membrane in phosphate buffer containing $FeCl_2$ was taken as a reference, and a series of SEIRA difference spectra was collected while adding H_2O_2. Negative peaks in the υ (CH_n) region (3000–2800 cm^{-1}) were observed, and their intensities gradually increased with time (Figs. 4(A-c) and (B-c)). A weak but discernible positive peak assigned to υ ($C=O$) appeared at 1745 cm^{-1}. Attenuation and eventual fusion of this peak with the negative peak at 1725 cm^{-1} was observed as the intensity of the negative peak of υ (CH_n) at 3000–2800 cm^{-1} increased. The significant difference in the positions of these two peaks corresponding to υ ($C=O$) suggests that they are located in different hydration microenvironments [36]. According to the Russell mechanism, the generation of $^1O_2$ during •OH-induced lipid peroxidation is accompanied by the formation of PS=*O*, whose carbonyl group is located inside the hydrophobic region of the membrane. Thus, the peak at 1747 cm^{-1} was tentatively assigned to the υ ($C=O$) of PS=*O*, and the peak at 1725 cm^{-1} was assigned to the υ ($C=O$) of the ester group in the alkyl chain of the lipid, which would have a higher degree of hydration. The occurrence of the υ ($C=O$) peak of PS=*O* further proves the generation of $^1O_2$. The simultaneous appearance of the negative peaks in the υ (CH_n) and υ ($C=O$) regions of the alkyl chain and the progressive increase in their intensities with time as observed through SEIRA spectroscopy indicates the migration of the lipid away from the enhancing substrate [37]. This phenomenon might be induced by the increase in polarity of the lipid alkyl chain due to the oxidation of $^1O_2$ and •OH, which results in the migration of lipid molecules into the aqueous phase and an increase in the membrane defect density, causing further loss of membrane integrity [38]. Therefore, the intensity of the negative peak at υ (CH_n) could be a reporter of membrane damage.

To further investigate the effect of $^1O_2$ and the resultant lipid peroxidation propagation on the membrane structure, a series of SEIRA difference spectra was collected after adding H_2O_2 mixed with NaN_3 using the spectrum of PS or PS/Ch membrane in phosphate buffer containing $FeCl_2$ as a reference. The overall change in the characteristic peaks of the membrane was similar to that without NaN_3. However, the intensities of the negative peaks due to lipid peroxidation showed distinct differences (Figs. 4A and B, d). It should be noted that NaN_3 had no effect on the conformation of the PS and PS/Ch membranes and did not affect the interaction of Fe^{2+} with the membranes (Fig. S10). The influence of $^1O_2$ generated during lipid peroxidation on the structure of the lipid membrane was investigated by comparing the membrane damage induced in the presence and absence of NaN_3, a specific $^1O_2$ quencher. The absolute value of the intensity ratio (I/I_0) of υ_{as} (CH_2) of the PS membrane before (I_0, positive peak) and after (I, negative peak) peroxidation was used to represent the membrane damage. As shown in Figs. 4(C) and (D), the value of I/I_0 is reduced by nearly 50% in the presence of NaN_3, indicating that $^1O_2$ produced from lipid peroxidation induces membrane damage with the exception of •OH. Nearly 50% of membrane damage was induced by the generation and propagation of $^1O_2$, and the depletion of $^1O_2$ only reduced the total ROS of the membrane by 20% (Fig. S9), suggesting that the propagation of $^1O_2$ and its oxidation are more likely to cause membrane damage. A recent study has reported that lipid cross-linking might be a particular event driving ferroptosis [39]. Our research further points to this molecular event, which could be a factor influencing ferroptosis.

Furthermore, the generation of $^1O_2$ and the resultant effect during ferroptosis were examined at the cellular level. Erastin, a ferroptosis activator, was used to trigger ferroptosis in A549 lung cancer cells [40].

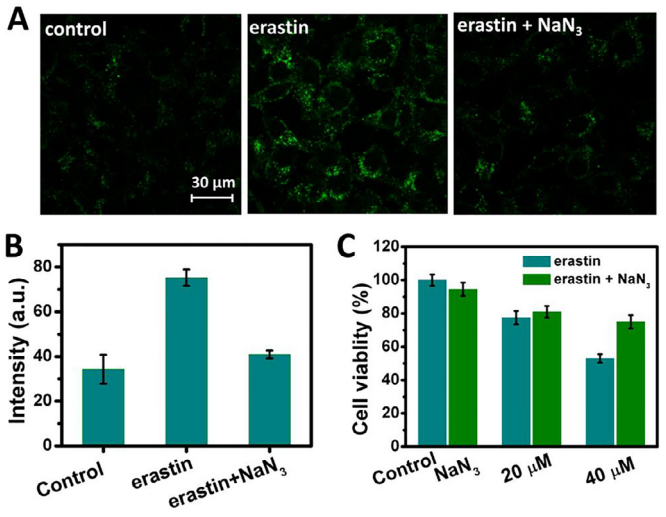

Fig. 5. (A) Confocal laser scanning fluorescence microscope (CLSM) images of SOSG-stained A549 cells treated with DMSO, erastin, and erastin with NaN_3 (B) and corresponding fluorescence intensity. (C) Cell viability of A549 cells treated with DMSO, erastin, and erastin with NaN_3. The viability assessment of cells treated with NaN_3 alone is also included as control.

Cell viability of A549 lung cancer cells after incubation with different concentrations of erastin was evaluated by using a standard MTT assay. The cell survival rate gradually decreased with an increase in the concentration of erastin (Fig. S11(A)). The addition of deferoxamine (DFO), an iron chelator [13], alleviated erastin-induced cell death (Fig. S11(B)), which confirms that A549 cells undergo ferroptosis induced by erastin. The generation of $^1O_2$ in erastin-treated cells was detected by SOSG using CLSM. Brighter green fluorescence of SOSG was observed in erastin-treated cells compared with that of untreated cells, and nearly the same fluorescence was observed for untreated cells and cells treated with erastin and NaN_3 (shown in Figs. 5(A) and (B)). These results suggest that $^1O_2$ is generated in erastin-treated cells upon ferroptosis. Moreover, the influence of the generated $^1O_2$ on cell viability during ferroptosis was investigated. As shown in Fig. 5C, cell viability can be recovered when the generated $^1O_2$ is depleted with NaN_3. This result indicates that the generated $^1O_2$ promotes ferroptosis.

Lipid peroxidation is a complex biochemical process that consists of a set of radical-mediated chain reactions, including initiation, propagation, and termination. Although different species have been used as chain initiators, the specific initiator of lipid peroxidation is yet to be identified [15]. Our study on the Fenton-reagent-triggered lipid peroxidation suggests that PS peroxidation might be initiated by the direct removal of a hydrogen atom from the allyl carbon by •OH, resulting in the generation of carbon-centered PS radicals (PS•), which subsequently react with O_2 to form PS peroxyl radicals (PS-OO•) (Fig. 6). PS-OO• can abstract hydrogen from neighboring PS lipids, leading to the formation of PS-OOH and PS• in addition to their enzymatic conversion to PS-OOH [8]. In the presence of iron cations, the produced PS-OOH can be decomposed into more reactive species such as PS-OO•, alkoxyl radicals (PS-O•), and epoxy radicals (OPS•), which further react with O_2 to form epoxyperoxyl radicals (OPSOO•) in the absence of GPX4. These species, as well as pre-formed PS•, can further abstract H-atoms from lipids to propagate lipid peroxidation chain reactions. Although •OH was reported to contribute the majority of the total ROS during ferroptosis [13], our results clearly show that in addition to lipid ROS, another reactive species, $^1O_2$ is generated from the self-reaction of two peroxy radicals (PS-OO•) accompanied by the formation of PS-OH and PS=*O* through the Russell mechanism. The generated $^1O_2$ can further propagate the lipid peroxidation chain reaction and the reaction governed by the Russell mechanism, leading to the significant accumulation of lipid ROS and subsequent damage to membrane integrity. These results suggest that the longstanding view that interaction between two peroxyl radicals serves as the termination step of lipid peroxidation [23] should be re-considered, and provide new insight into both lipid peroxidation and ferroptosis.

4. Conclusion

This is the first study in which the molecular mechanism of singlet oxygen generation and its influence on ferroptosis were investigated. At the molecular level, hydroxyl radicals produced by the Fenton reaction were found to induce lipid peroxidation to yield lipid peroxy radicals, which can not only interact with surrounding lipids to propagate the peroxidation reaction, producing an abundance of lipid peroxy radicals and hydroperoxides, but also generate a certain amount of singlet oxygen through the Russell mechanism. Furthermore, under the catalytic effect of iron cations, lipid hydroperoxides and lipid peroxy radicals can generate a large amount of singlet oxygen via the Russell mechanism in an iron cation-dependent chain reaction pathway, which results in accelerated propagation and serious accumulation of lipid ROS, ultimately damaging the membrane integrity regardless of the presence of cholesterol. At the cellular level, we observed that ferroptosis triggered

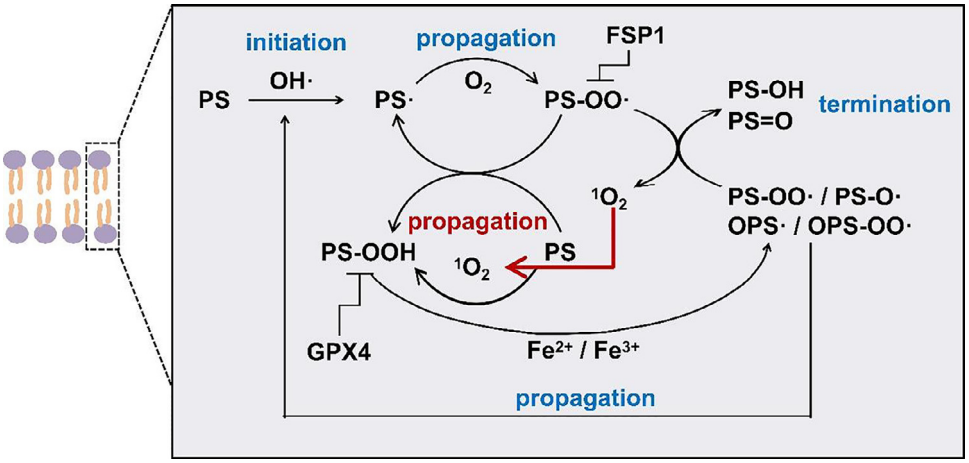

Fig. 6. Overview of proposed reaction pathway of lipid peroxidation and generation of $^1O_2$. GPX4 catalyzes the reduction of hydroperoxides to their corresponding alcohols and detoxification of PS-OOH. FSP1 suppresses lipid peroxidation by reducing ubiquinone to ubiquinol, which in turn may directly reduce lipid radicals to terminate lipid autoxidation.

by erastin is accompanied by the generation of $^1O_2$, which further promotes cell death. This discovery provides an in-depth insight into ferroptosis and can be potentially utilized in the treatment of related diseases and design of targeted drugs.

Declaration of Competing Interest

The authors declare that they have no conflicts of interest in this work.

Acknowledgments

This work was financially supported by the National Science Fund for Distinguished Young Scholars (Grant No. 22025406), the National Natural Science Foundation of China (Grants No. 21874125, 22074138), Science and Technology Innovation Foundation of Jilin Province (Grants No. 20190201074JC, 20200703021ZP), and the Youth Innovation Promotion Association of CAS (Grant No. 2020233).

Supplementary materials

Supplementary material associated with this article can be found, in the online version, at doi:10.1016/j.fmre.2021.07.008.

References

[1] D.L. Vaux, S.J. Korsmeyer, Cell death in development, Cell 96 (2) (1999) 245–254.
[2] S.J. Dixon, K.M. Lemberg, M.R. Lamprecht, et al., Ferroptosis: an iron-dependent form of non-apoptotic cell death, Cell 149 (5) (2012) 1060–1072.
[3] J. Li, F. Cao, H.L. Yin, et al., Ferroptosis: past, present and future, Cell Death Dis 11 (2) (2020) 88.
[4] Y. Xie, W. Hou, X. Song, et al., Ferroptosis: process and function, Cell Death Differ 23 (3) (2016) 369–379.
[5] W.S. Yang, R. SriRamaratnam, M.E. Welsch, et al., Regulation of ferroptotic cancer cell death by GPX4, Cell 156 (1) (2014) 317–331.
[6] L. Jiang, N. Kon, T.Y. Li, et al., Ferroptosis as a p53-mediated activity during tumour suppression, Nature 520 (7545) (2015) 57–62.
[7] J.Y. Cao, S.J. Dixon, Mechanisms of ferroptosis, Cell. Mol. Life Sci. 73 (11) (2016) 2195–2209.
[8] X. Jiang, B.R. Stockwell, M. Conrad, Ferroptosis: mechanisms, biology and role in disease, Nat. Rev. Mol. Cell Biol. 22 (4) (2021) 266–282.
[9] H. Feng, B.R. Stockwell, Unsolved mysteries: how does lipid peroxidation cause ferroptosis? PLoS Biol 16 (5) (2018) e2006203.
[10] D.A. Stoyanovsky, Y.Y. Tyurina, I. Shrivastava, et al., Iron catalysis of lipid peroxidation in ferroptosis: regulated enzymatic or random free radical reaction? Free Radical Biol. Med. 133 (2019) 153–161.
[11] W.S. Yang, K.J. Kim, M.M. Gaschler, et al., Peroxidation of polyunsaturated fatty acids by lipoxygenases drives ferroptosis, Proc. Natl. Acad. Sci. U. S. A. 113 (34) (2016) E4966–E4975.
[12] V.E. Kagan, G. Mao, F. Qu, et al., Oxidized arachidonic and adrenic PEs navigate cells to ferroptosis, Nat. Chem. Biol. 13 (1) (2017) 81–90.
[13] H. Li, W. Shi, X. Li, et al., Ferroptosis accompanied by •OH generation and cytoplasmic viscosity increase revealed via dual-functional fluorescence probe, J. Am. Chem. Soc. 141 (45) (2019) 18301–18307.
[14] J.P.F. Angeli, R. Shah, D.A. Pratt, et al., Ferroptosis inhibition: mechanisms and opportunities, Trends Pharmacol. Sci. 38 (5) (2017) 489–498.
[15] Z. Cheng, Y. Li, What is responsible for the initiating chemistry of iron-mediated lipid peroxidation: An update, Chem. Rev. 107 (3) (2007) 748–766.
[16] J.A. Howard, K.U. Ingold, Self-reaction of sec-butylperoxy radicals. Confirmation of the Russell mechanism, J. Am. Chem. Soc. 90 (4) (1968) 1056–1058.
[17] E. Choe, D.B. Min, Chemistry and reactions of reactive oxygen species in foods, J. Food Sci. 70 (9) (2005) R142–R159.
[18] C. Tian, J. Li, Q. Li, et al., Surface weak acid-base pair of FeOOH/Al_2O_3 for enhanced peroxymonosulfate activation in degradation of humic substances from water, Chem. Eng. J. 387 (2020) 124064.
[19] M.J. Glade, K. Smith, Phosphatidylserine and the human brain, Nutrition 31 (6) (2015) 781–786.
[20] S.G. Kathman, J. Boshart, H. Jing, et al., Blockade of the lysophosphatidylserine lipase ABHD12 potentiates ferroptosis in cancer cells, ACS Chem. Biol. 15 (4) (2020) 871–877.
[21] X. Zhang, K.M. Barraza, J.L. Beauchamp, Cholesterol provides nonsacrificial protection of membrane lipids from chemical damage at air–water interface, Proc. Natl. Acad. Sci. U. S. A. 115 (13) (2018) 3255–3260.
[22] L. Iuliano, Pathways of cholesterol oxidation via non-enzymatic mechanisms, Chem. Phys. Lipids 164 (6) (2011) 457–468.
[23] H. Yin, L. Xu, N.A. Porter, Free radical lipid peroxidation: mechanisms and analysis, Chem. Rev. 111 (10) (2011) 5944–5972.
[24] W.Y. Tai, Y.C. Yang, H.J. Lin, et al., Interplay between structure and fluidity of model lipid membranes under oxidative attack, J. Phys. Chem. B 114 (47) (2010) 15642–15649.
[25] S. Miyamoto, G.R. Martinez, M.H.G. Medeiros, et al., Singlet molecular oxygen generated from lipid hydroperoxides by the Russell mechanism: Studies using ^{18}O-labeled linoleic acid hydroperoxide and monomol light emission measurements, J. Am. Chem. Soc. 125 (20) (2003) 6172–6179.
[26] F.F. Hsu, J. Turk, Studies on phosphatidylserine by tandem quadrupole and multiple stage quadrupole ion-trap mass spectrometry with electrospray ionization: structural characterization and the fragmentation processes, J. Am. Soc. Mass Spectrom. 16 (9) (2005) 1510–1522.
[27] J. Kim, C.L. Hoppel, Identification of unusual phospholipids from bovine heart mitochondria by HPLC-MS/MS, J. Lipid Res. 61 (12) (2020) 1707–1719.
[28] X. Zhang, K.M. Barraza, K.T. Upton, et al., Subtle changes in lipid environment have profound effects on membrane oxidation chemistry, J. Am. Chem. Soc. 140 (50) (2018) 17492–17498.
[29] P.D. Piehowski, A.J. Carado, M.E. Kurczy, et al., MS/MS methodology to improve subcellular mapping of cholesterol using TOF-SIMS, Anal. Chem. 80 (22) (2008) 8662–8667.
[30] G.E. Ronsein, F.M. Prado, F.V. Mansano, et al., Detection and characterization of cholesterol-oxidized products using HPLC coupled to dopant assisted ttmospheric pressure photoionization tandem mass spectrometry, Anal. Chem. 82 (17) (2010) 7293–7301.
[31] M. Uemi, G.E. Ronsein, F.M. Prado, et al., Cholesterol hydroperoxides generate singlet molecular oxygen [O_2 ($^1\Delta_g$)]: near-IR emission, ^{18}O-labeled hydroperoxides, and mass spectrometry, Chem. Res. Toxicol. 24 (6) (2011) 887–895.
[32] A.W. Girotti, Lipid hydroperoxide generation, turnover, and effector action in biological systems, J. Lipid Res. 39 (8) (1998) 1529–1542.
[33] G.P.C. Drummen, L.C.M. van Liebergen, J.A.F. Op den Kamp, et al., C11-BODIPY581/591, an oxidation-sensitive fluorescent lipid peroxidation probe: (micro)spectroscopic characterization and validation of methodology, Free Radical Biol. Med. 33 (4) (2002) 473–490.
[34] N. Kitadai, T. Yokoyama, S. Nakashima, ATR-IR spectroscopic study of L-lysine adsorption on amorphous silica, J. Colloid Interface Sci. 329 (1) (2009) 31–37.
[35] C.Y. Tang, Z. Huang, H.C. Allen, Binding of Mg^{2+} and Ca^{2+} to palmitic acid and deprotonation of the COOH headgroup studied by vibrational sum frequency generation spectroscopy, J. Phys. Chem. B 114 (51) (2010) 17068–17076.
[36] I. Zawisza, A. Lachenwitzer, V. Zamlynny, et al., Electrochemical and photon polarization modulation infrared reflection absorption spectroscopy study of the electric field driven transformations of a phospholipid bilayer supported at a gold electrode surface, Biophys. J. 85 (6) (2003) 4055–4075.
[37] L. Wu, L. Zeng, X. Jiang, Revealing the nature of interaction between graphene oxide and lipid membrane by surface-enhanced infrared absorption spectroscopy, J. Am. Chem. Soc. 137 (32) (2015) 10052–10055.
[38] R. Itri, H.C. Junqueira, O. Mertins, et al., Membrane changes under oxidative stress: the impact of oxidized lipids, Biophys. Rev. 6 (1) (2014) 47–61.
[39] V.A.N. Kraft, C.T. Bezjian, S. Pfeiffer, et al., GTP cyclohydrolase 1/tetrahydrobiopterin counteract ferroptosis through lipid remodeling, ACS Cent. Sci. 6 (1) (2020) 41–53.
[40] C. Huang, M. Yang, J. Deng, et al., Upregulation and activation of p53 by erastin-induced reactive oxygen species contribute to cytotoxic and cytostatic effects in A549 lung cancer cells, Oncol. Rep. 40 (4) (2018) 2363–2370.

Xiaofei Zhang obtained her PhD degree in University of Science and Technology of China in 2020. She works now at Changchun University. Her major research interest focuses on the molecular mechanism of biological effect induced by nano scale materials.

Xiue Jiang, Professor at the Changchun Institute of Applied Chemistry, Chinese Academy of Science, Changchun, China. Received her PhD in 2005 from Changchun Institute of Applied Chemistry. Then worked as an Alexander von Humboldt Research Fellowship at Bielefeld University (Germany), a Postdoctoral Fellow at Ulm University (Germany). Since 2010, Xiue has been a Full Professor at the Changchun Institute of Applied Chemistry, Chinese Academy of Science. Her current research interests mainly contain revealing the weak interaction at the interface of cellular membrane and the regulation function of water, and revealing the cellular response mechanisms at the nanoscale by various spectroscopy methods, especially surface-enhanced infrared spectroscopy, for biomedical applications. She has published over 80 scientific papers and has holded 5 patents. Dr. Jiang is a recipient of the “National Science Fund for Excellent Young Scholars in China” and “National Science Fund for Distinguished Young Scholars in China”. She is editorial board member of Fundamental Research.